# Chapter 3
# INSTRUMENTATION

## HISTORICAL BACKGROUND

The historical evolution of solar radiation measurement is deserving of brief mention, so some of the early pioneers of solar research and their instruments will be described here. Sir William Herschel in England and the Frenchman Pouillet independently developed the actinometer in the early 1800's for performing quantitative measurements of direct solar irradiance. Systematic solar radiation measurements were begun by Pouillet in France in 1838 [*Abbot, 1926*].

In the United States John Ericsson devised a calorimeter which could be used to measure the temperature rise of a known mass of water in an insulated container. On a clear summer day in New York in 1876 Ericsson measured the direct solar irradiance all day and by extrapolation determined the solar irradiance outside the Earth's atmosphere to be 1345 W/m$^2$. His result is within 2% of the presently accepted value for the solar constant.

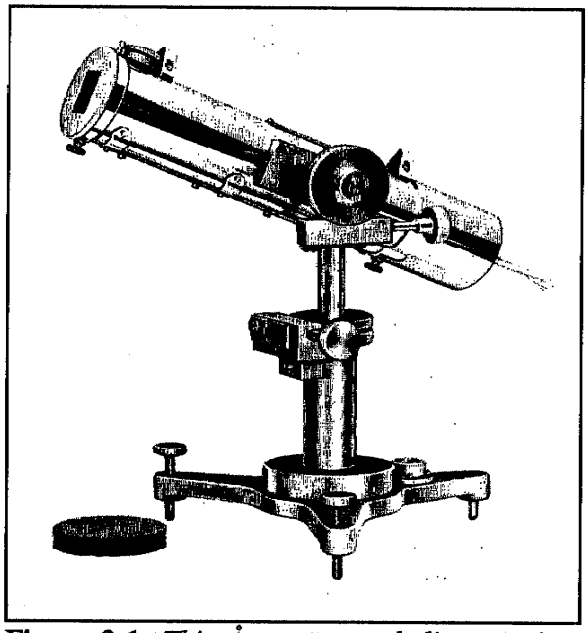

**Figure 3.1:** *This Ångström pyrheliometer is an improved Eppley version from 1974.*

Samuel Pierpont Langley, third Secretary of the Smithsonian Institution in Washington began measurements of the spectral distribution of solar radiation in the early 1880's. His instrument was a bolometer invented in 1878 which used a very thin strip of blackened platinum in one arm of a Wheatstone bridge. By moving the strip across a meter-long solar spectrum from a large spectrometer he was able to measure the spectral irradiance of the Sun for a range of solar elevation angles. In connection with this work he discovered the portion of the spectrum beyond 800 nanometers, i.e. the near infrared portion of the solar spectrum [*Yellott, 1977, p III-3; Langley, 1886*].

The Ångström pyrheliometer (Figure 3.1) was invented in 1893 by K.J. Ångström (son of the Swedish astronomer for whom the Ångström unit is named). The heart of the instrument is two thin, narrow blackened strips of manganin placed side by side at the bottom of a collimating tube. A carefully regulated DC current could be passed through one of these strips while the other was exposed to the Sun. Thermo-

Figure 3.3 shows a model calculation based on this geometry for the instruments which we built for use at Thule Air Base:

| | |
|---|---|
| Detector diameter | 2 mm |
| Aperture diameter | 10 mm |
| Detector-aperture distance | 260 mm |

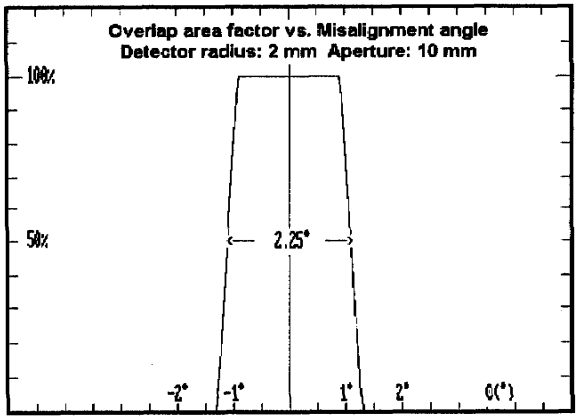


**Figure 3.3:** *Model calculation of expected SolData pyrheliometer directional responsivity.*

The FOV as measured between the 50% sensitivity points is 2.25°. The total angular range within which the detector is completely exposed is 1.76°, and the total slope angle within which the detector is partly exposed is 0.88°. Figures 3.4 and 3.5 show actual measurements performed on a SolData pyrheliometer using a small halogen lamp (effectively a point source) placed at a distance of 10 meters from the instrument.

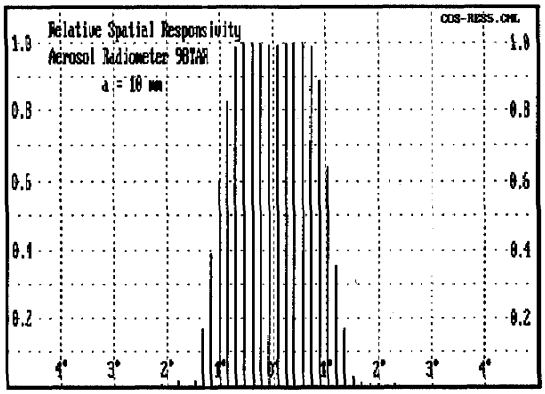


**Figure 3.4:** *Directional responsivity measurements for SolData pyrheliometers.*

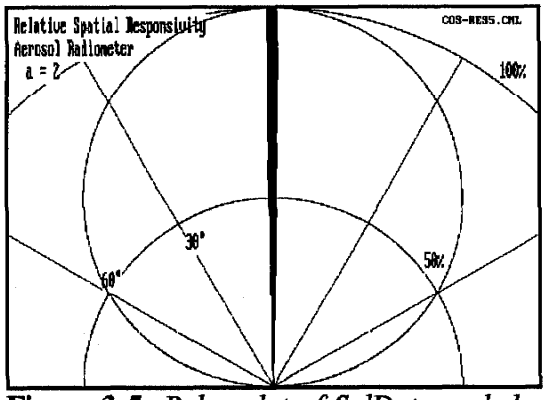


**Figure 3.5:** *Polar plot of SolData pyrheliometer directional responsivity.*

The Dexter Model 2M thermopile is mounted in a TO-5 housing and exhibits flat response from the UV to the far infrared. The spectral response is limited, however, to 300-3000 nm by the sapphire window protecting the thermopile. The responsivity is specified to be 20 V/W and to be linear from $10^{-6}$ to $10^{-1}$ W/cm$^2$.

The responsivity was confirmed by exposure to sunlight and found to be about 80 mV under direct solar illumination (100 mW/cm$^2$). Detector linearity over four decades was confirmed by testing it with a range of neutral density filters. The Dexter 2M detector signal was amplified using an instrumentation amplifier, so that the resulting instrument signal was about 900 mV under full solar illumination at air mass 1.5. The detector housing and electronics were temperature regulated, so that the operating temperature was 20±½°C throughout the period of operation. This instrument is referred to as the *SolData 2M pyrheliometer*.

## MECHANICAL DETAILS

Figure 3.6 shows an overview diagram of the mechanical configuration of the Sol-Data pyrheliometer design (without the climate shield).

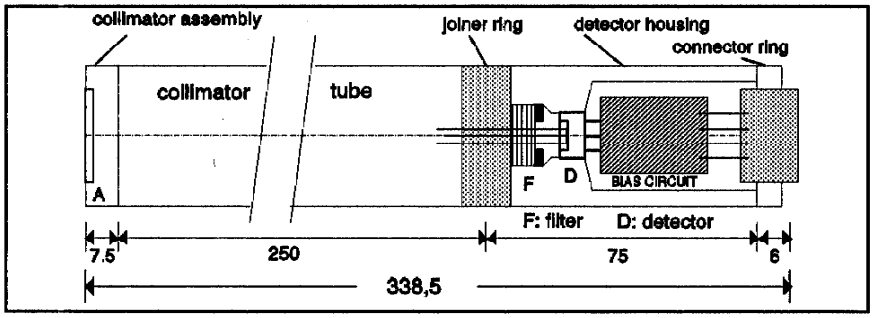


**Figure 3.6:** *The overall mechanical configuration of the SolData pyrheliometers (both broad-band and filter) is shown here.*

The SolData 2M pyrheliometer, broad-band instrument uses no filter, and the Dexter 2M detector package is mounted in a standard TO-5 housing (Figure 3.7) with a sapphire window. It has a 2 x 2 mm sensitive area. The 500 nm and 1030 nm instruments have the configuration shown in Figure 3.8 showing the detector-filter assembly with an interference filter and a Hamamatsu type 6626 photodiode. The 6626 photodiode dimensions are seen in this illustration (detector area 2.4 x 2.8 mm). Finally the 1550 nm instrument used a Hamamatsu G5114-02 InGaAs photodiode with a 2.0 mm diameter active area.

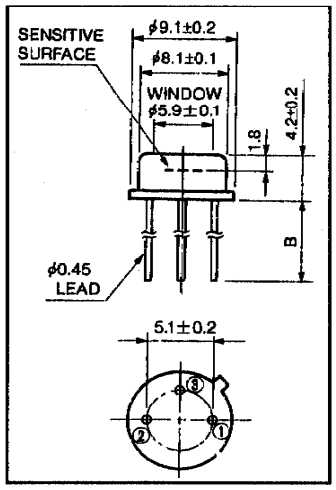


**Figure 3.7:** *TO-5 housing.*

Figure 3.9 shows details of the aperture assembly. The 10 mm collimator aperture was identical for all four SolData pyrheliometers. The aperture was protected from the elements by a 2 mm thick glass cover.

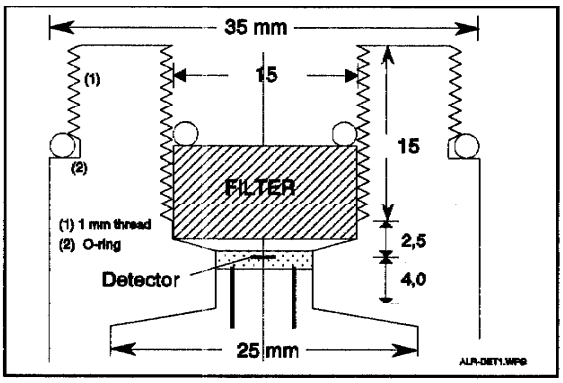


**Figure 3.8:** *The detector housing contains the photodetector and electronics and is mounted at the base of the collimator tube.*

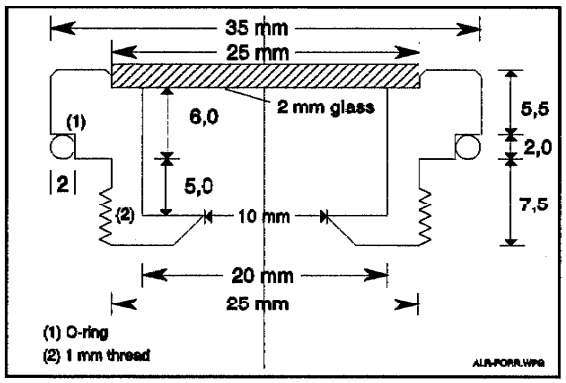


**Figure 3.9:** *The aperture assembly used with the SolData pyrheliometers is mounted on the front of the collimator tube.*

The mechanical assembly shown in Figure 3.6 was prepared as follows for mounting at Thule Air Base:

- A Minco Corporation type HK15228 Thermofoil 51 x 102 mm heater (controller type CT198-2) was mounted on the outer surface of the cylindrical detector housing. The two heater wires passed through a small hole inside the housing where they were connected along with the supply power, output signal and temperature sensor wires to the 8-pole "Mini-Buccaneer IP68" weatherproof female connector.
- Two plexiglas mounting rings were machined and prepared with two 4 mm set screws, so that they could be mounted securely at the aperture end and at the connector end of the pyrheliometer assembly. At the bottom of each ring 4 mm galvanized bolts protruded for securing the assembly to the climate shield.
- Strips of polyurethane foam insulation were wrapped around the 35 mm diameter detector housing and collimator assembly to provide a total thickness of about 4 millimeters of foam insulation.
- A 50 mm diameter outer diameter aluminum tube served as a climate shield (with a flat black inner surface and white outer surface). A 4.5 mm slit at the bottom allowed the shield to be slid down over the pyrheliometer and fastened securely using the two 4 mm bolts protruding from the plexiglas rings. The slit and bolt method is apparent from Figure 3.10.

**Figure 3.10:** *The photograph shows the four SolData pyrheliometers (2M, 500, 1030 and 1550 nm) mounted within the climate shields, and the Kipp-Zonen 368 nm pyrheliometer at the lower right.*

- The pyrheliometer cable was five meter long 10-lead PVC-clad shielded cable with 8 pole male mini-Buccaneer connectors at both ends. The cable was connected to a power supply and connector assembly from which the pyrheliometer output signals were passed to the data logger.

- The pyrheliometers were connected in pairs to the SciTec 2AP belt driven two-axis solar tracker using specially prepared mounting brackets produced at the DMI machine shop. Software and other accessories for the tracker were in place at the Thule Air Base laboratory.

The final tracker assembly with all five pyrheliometers in place can be seen in Figure 3.10. This experimental setup permitted continuous tracking of the Sun with the Kipp-Zonen 368 pyrheliometer, the SolData 500, 1030 and 1550 nm pyrheliometers plus the SolData 2M pyrheliometer. The experiment operated with a minimum of interruptions from May 15th through October 4th, 1999.

## DETECTOR AND ELECTRONICS

An noted the 500 and 1030 nm instruments employed a Hamamatsu type S6626 silicon photodiode. This device has a flat 2.4 mm x 2.8 mm photosensitive surface area and could be readily mounted in the detector housing. The spectral response of a typical silicon photodiode of this type is shown in Figure 3.11. Ferroperm Optics A/S interference filters (10 nm FWHM bandwidth) were used in conjunction with the silicon detector to provide the desired spectral response for the instruments. The 1550 nm near infrared pyrheliometer employed an interference filter produced by Andover Corporation with a 10 nm bandwidth and a Hamamatsu InGaAs detector.

The photodiodes were connected in photovoltaic mode to an operational amplifier (current-to-voltage converter) with feedback resistors selected to provide output signals when exposed to air mass 1.5 sunshine of about 900 mV. A capacitor across the feedback resistor was chosen to reduce noise while not compromising response time. We aimed for a response time of about 100 ms. As will subsequently be seen from our data there was slight overshoot (excess of 1000 mV to the data logger) from the 500 nm instrument during a few midsummer weeks at Thule Air Base, while the other instruments performed within the acceptable output signal range as planned.

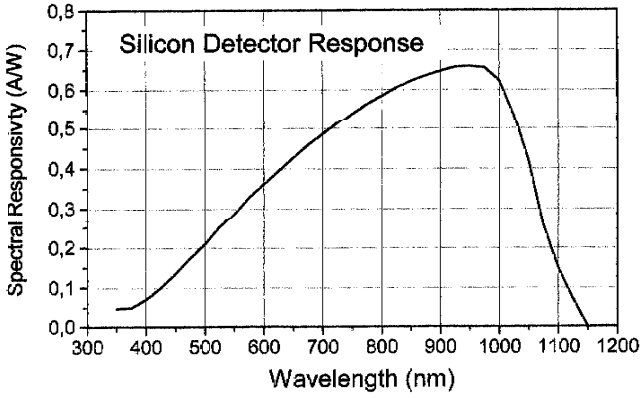


**Figure 3.11:** *Typical silicon photodiode spectral responsivity is shown.*

For the SolData 2M pyrheliometer an amplifier was constructed from two operational amplifiers on a single chip, with the second op amp configured as an invertor to provide a positive output signal. An LM35DZ temperature sensor chip was

mounted on the electronics board to monitor detector housing temperature. The Minco heater held the temperature constant at 20°C to within about ±½°C throughout the course of the experiment.

The photodiodes in the SolData filter pyrheliometers are employed in photovoltaic configuration (unbiased). This mode is preferred for low frequency and low light level applications, and manufacturers' specifications show less responsivity change with temperature than photoconductive mode applications [*UDT Sensors Catalog, p 10*]. Tests conducted during instrument construction showed that temperature changes had a significant influence on the output signals for all pyrheliometers, with the 1030 nanometer instrument being most sensitive to temperature change. Figure 3.12 shows temperature coefficients of about –0.2%/°C for silicon photodiodes in the 500-900 nm range followed by a rapid increase to +2%/°C above 1000 nm. The high sensitivity to temperature changes at wavelengths from 900-1100 nm can be understood by viewing the silicon spectral responsivity shown in Figure 3.11. The responsivity graph is quite steep in this region so that small temperature changes can have significant effects.

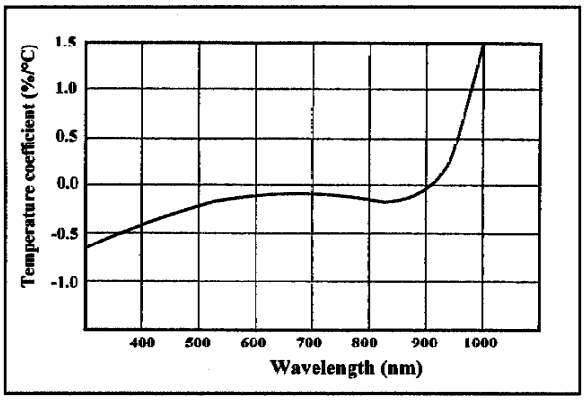


**Figure 3.12:** *Typical silicon detector temperature coefficient vs. wavelength.*

Interference filters centered within the wavelength range from 400-1550 nm are reported to have a temperature coefficient of 0.015 increasing to 0.035 nm/°C within this range [*Andover Corporation Filter Guide, p 18*]. It is therefore very important to insure temperature stability using the Minco heater solution described earlier.

At zero signal levels noise signals from the SolData pyrheliometers were higher than the noise from the Kipp-Zonen pyrheliometer. This could be reduced by mounting the power supply and connector terminals to the data logger inside a sealed metal case instead of using the open terminal strip for making connections. When in operation with full solar illumination the noise was insignificant and did not interfere with the measurements.

## WEATHER STATION

A set of instruments for monitoring weather parameters was available at the Thule Air Base laboratory. The parameters available were:

- ambient outdoor temperature
- wind speed
- wind direction
- relative humidity

In addition a Yankee Environmental Systems ventilated pyranometer provided information about the short wave global irradiance on a horizontal surface.

## CCD SPECTROMETER

A CVI Spectral SM-210 CCD spectrometer (*sn: 1V1-0053*) similar to the instrument shown in Figure 3.7 was used to perform direct solar spectral irradiance measurements for comparison with filter pyrheliometer data. Because the spectrometer setup was not prepared for long term automation, it was not mounted at the Thule Air Base laboratory but used instead for measurements in Silkeborg, Denmark. This discussion can be regarded as a feasibility study intended to provide helpful information for future users of the instrument, perhaps at Thule Air Base.

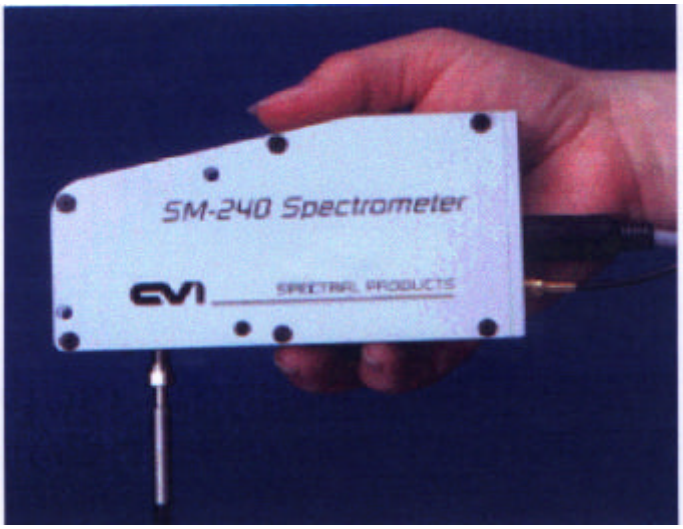


**Figure 3.13:** *A CCD spectrometer with a fiber optic probe mounted on an Eppley tracker was used to obtain solar spectra in Silkeborg, Denmark.*

| | | | |
|---|---|---|---|
| size: | 140 x 70 x 22 mm | slit width: | 100 μm |
| mass: | 250 grams | numerical aperture: | 0.20 |
| spectral range: | 380-760 nm | dynamic range: | 12 bit (4096:1) |
| spectral resolution: | 2.5 nm (100 μm slit) | PC interface: | ISA/PCMCIA |
| f-number: | 3.3 | CCD element size: | 14 x 14 μm |
| entrance aperture: | SMA coupler for FO | Operating temperature: | 0°C - 40°C |

**Table 3.1:** *Specifications for the CVI-Spectral 1024 channel CCD spectrometer.*

The physical CCD array contains 2048 pixels, but the SM-210 software provides only 1024 spectrometer channels. The length of the CCD is about 30 mm.

Two calibration procedures are required in order to reduce the raw CCD pixel data to solar spectra. The first is *wavelength* calibration vs. pixel number, and the second is *relative spectral irradiance* vs. the measured system response for a given spectrometer channel.

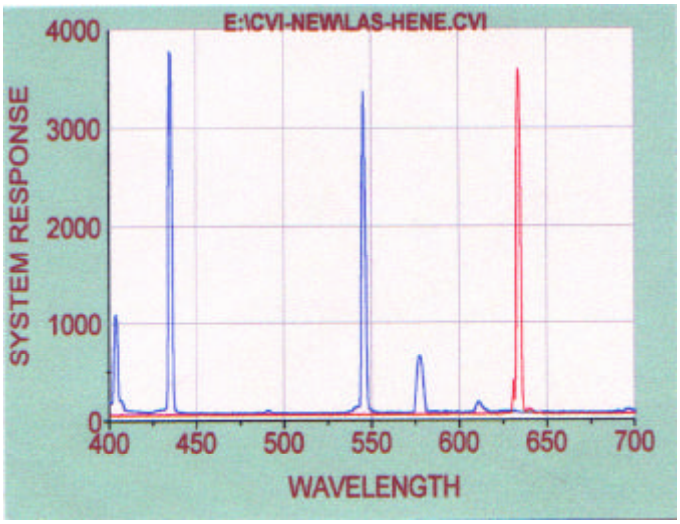


**Figure 3.14:** *The CVI spectrometer wavelength calibration was checked using a mercury vapor lamp (blue) and HeNe laser (red).*

### WAVELENGTH CALIBRATION

The preliminary calibration had been performed at the factory, and it was checked against a *He-Ne* laser and

spectral lines from a mercury vapor lamp as shown in Figure 3.14. The spectrometer was cross-checked where possible with some of the narrow band interference filters to be used in the optical depth experiments. These checks were in accord with the manufacturer's data and accurate to $\pm 1$ nm. The following algorithm could be used to fit *wavelength* $\lambda$ to *pixel number* $p$. A second order polynomial was adequate to determine the wavelength as a function of pixel number.

$$\lambda = 8.97268 \cdot 10^{-5}\ p^2 + 0.630553\ p + 306.539 \qquad (3.1)$$

Spectrometer linearity was checked at selected wavelengths by means of a pair of neutral density filter wheels over four decades and found to be excellent.

## SPECTRAL IRRADIANCE CALIBRATION

Calibration of the spectrometer to correctly measure absolute or relative spectral irradiance is a non-trivial exercise. In our aerosol measurments it is in fact sufficient to have good linearity at each wavelength of interest to perform the analysis. However, for closer examinations of the solar spectrum this additional information is necessary.

When using the CCD spectrometer to acquire solar spectra, the first task is to design an appropriate optical detector to receive the radiation of interest, in this case direct solar irradiance. This was achieved by using an aluminum collimator with a 10 mm diameter aperture and a 260 mm aperture-detector distance corresponding to an aperture half angle of about 1.1°. This housing was identical to the filter pyrheliometer housing described earlier with the end of the CCD cable replacing the silicon photodiode.

Direct solar radiation at low air mass values has a high power level per unit area (ca. 100 mW/cm$^2$) so that using a lens with the proper focal length to match the numerical aperture of the fiber optic (FO) cable would cause saturation of the spectrometer CCD detector array. The numerical aperture

$$NA = \sin\theta = \sqrt{n_1^2 - n_2^2} \qquad (3.2)$$

where $\theta$ is the *half-angle* of the FO cable acceptance angle, $n_1$ is the *index of refraction* of the FO cable core, and $n_2$ is the *index of refraction* of the cable cladding.

An alternative solution was therefore adopted using an opal glass diffuser about 10 millimeters from the end of the FO cable. The forward scattering due to multiple scattering within the diffuser glass yields an approximately lambertian source as viewed from the cable aperture. Only radiation entering the cable within the viewing cone as determined by the numerical aperture then enters the FO cable for transmission to the spectrometer slit. This solution fed the incoming radiation uniformly to the cable and at the same time provided the necessary attenuation to avoid CCD saturation.

## INTERFERENCE FRINGING

The CVI SM-210 instrument used in our experiments was designed to detect radiation in the 380-760 nanometer range, i.e. primarily the visible region, although measurements are possible outside this range if care is exercised to avoid second order spectra. The quantum efficiency is of course affected by the characteristics of the silicon detector element, but other factors also play an important role. Radiation must penetrate the polysilicon gate structure before reaching the CCD sensing elements thus causing reduced photoresponse. Finally, undesired interference fringing can arise due to the multiple layer structures of the CCD such as oxide layers, polysilicon gate structures and bulk silicon [*Wang, 1987, p 849*]. Although later versions of the CVI instrument seek to avoid this problem by using coatings of appropriate refractive index to suppress these fringing effects, this was not the case for the *sn: ...53* instrument used in our work, but it is now available with newer model CVI spectrometers.

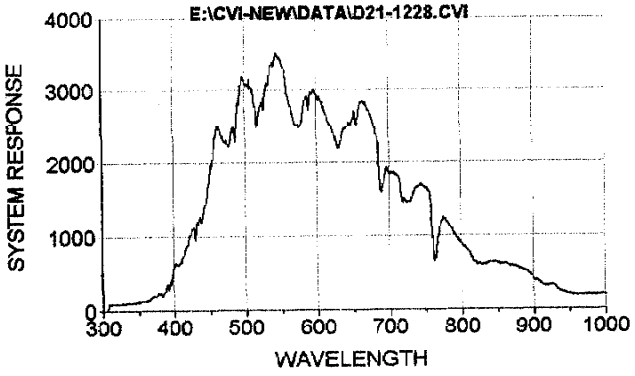


**Figure 3.15:** *This raw solar spectrum was acquired in Silkeborg around noon. Note the wavy structure due to interference fringing in the CCD.*

## CALIBRATION LAMP SPECTRA

Fringing effects and quantum efficiency variations in the CCD array combined with the optical characteristics of the opal diffuser and the FO cable all contribute to the resulting raw spectral signal shown in Figure 3.15. In order to calibrate the spectrometer and thus arrive at realistic representations of solar spectra, we have investigated a calibration method using high intensity incandescent lamps. The emission spectra from such lamps closely follows a Planck blackbody function:

$$I(\lambda) = \frac{2\pi \cdot h \cdot c^2}{\lambda^5} \frac{1}{e^{hc/\lambda kT} - 1} = \frac{c_1}{\lambda^5} \frac{1}{e^{c_2/\lambda T} - 1} \qquad (3.3)$$

where $c$ is the *speed of light* in a vacuum, $\lambda$ is the radiation *wavelength*, $k$ is *Boltzmann's constant*, $h$ is *Planck's constant* and $T$ is the *Kelvin temperature* of the source. The expression at the right in the above expression is useful for practical calculations. The values of the constants in SI units are:

$$c_1 = 3.741775 \cdot 10^{-16} \quad \text{and} \quad c_2 = 0.01438769$$

In passing we note that setting the first derivative of this function equal to zero yields a practical equation expressing the wavelength value at which the Planck curve has its maximum as a function of the source Kelvin temperature $T$:

$$\lambda_{MAX}(nm) = 2.90 \cdot 10^6 / T(K)$$

with the result in nanometers, and termed the *Wien displacement law*.

## INSTRUMENT FUNCTION

If a known spectral irradiance $I_C(\lambda)$ from a given source is measured in conjunction with a measurement run of solar spectra, then an instrument function $S(\lambda)$ can be determined as follows. Suppose that the raw calibration data acquired have the functional form $D_C(\lambda)$, while the known spectral irradiance should be $I_C(\lambda)$. The instrument function can be found as follows:

$$I_C(\lambda) = S(\lambda) \cdot D_C(\lambda)$$

$$S(\lambda) = I_C(\lambda)/D_C(\lambda) \quad \textbf{(3.4)}$$

Subsequent data $D(\lambda)$ collected in the same experimental setup can be corrected by applying the instrument function, so that the unknown spectral irradiance is obtained.

$$I(\lambda) = S(\lambda) \cdot D(\lambda) \quad \textbf{(3.5)}$$

Figure 3.16 shows raw calibration data from an incandescent halogen lamp with a radiant exitance of known color temperature typically around 3000 K, and Figure 3.17 shows the Planck curve for such a lamp. Finally Figure 3.18 shows a typical instrument function $S(\lambda)$ which can be subsequently applied to correct raw solar spectral data to obtain the spectral irradiance.

Notice the limitations in the instrument function for shorter wavelengths where the low UV content of the calibration lamp causes the signal to noise ratio to decrease. Due to the possibility of second order spectra, data above 760 nm must of course be viewed with caution or an appropriate blocking filter must be used.

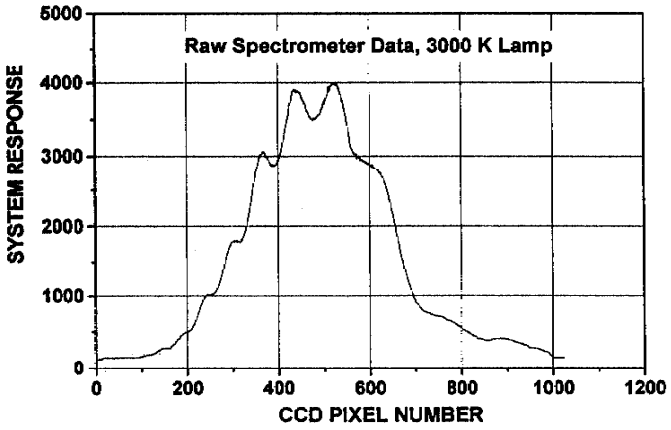


**Figure 3.16:** *The figure shows raw spectral data from a halogen calibration lamp (T ≈ 3000 K).*

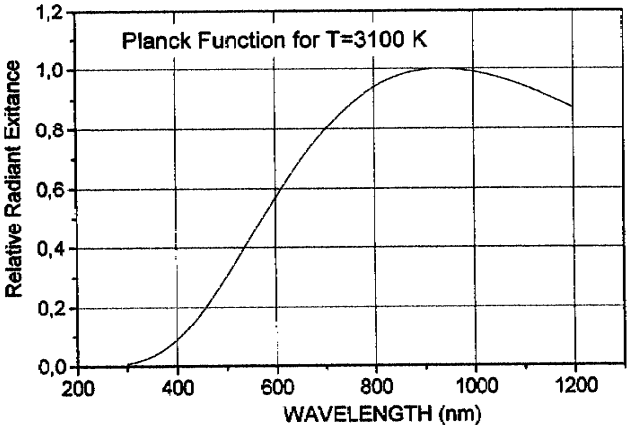


**Figure 3.17:** *The Planck curve for a 3100 K source. Note that the maximum exitance occurs at 935 nm (Wien's law).*

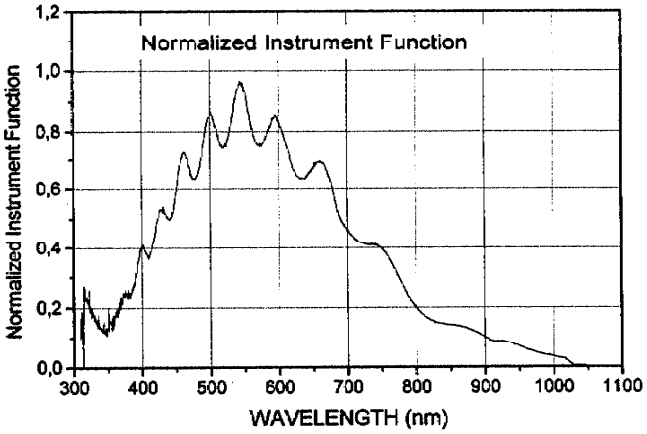


**Figure 3.18:** *Instrument function based on calibration lamp data and the assumption of Planck function radiant exitance.*

## COLOR TEMPERATURE MEASUREMENT

It should be noted of course that the assumed or measured value of the Planck temperature which characterized the lamp is of primary importance to this calibration scheme. We have therefore devoted some attention to the problem of finding the correct color temperature for a given light source. One method involves the use of Schott color filters (see Figure 3.19) with well-defined spectral transmittivity functions in conjunction with a pyrheliometer with known spectral response.

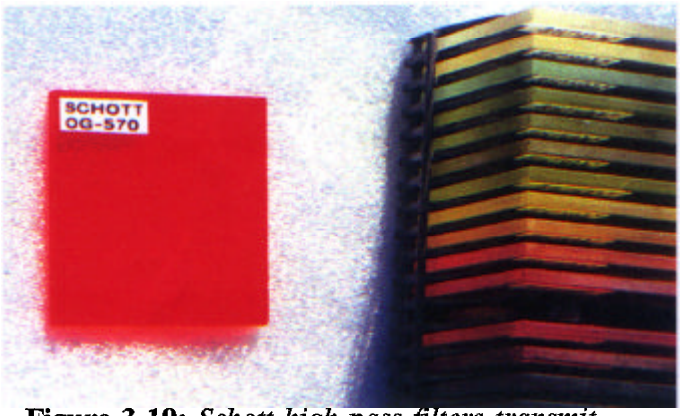


**Figure 3.19:** *Schott high-pass filters transmit radiation above a specified cutoff wavelength.*

Although the unit *lux* = *lumen/m²* would seem most suitable for use in the biological sciences, here is an example of how a high quality lux-meter can be used to find important physical quantities. The instrument employed for this analysis was a Hagner E2X (*sn: E20933X*) designed to closely follow the CIE (*Commission International d'Eclairage*) photopic response of the human eye, see Figure 3.20.

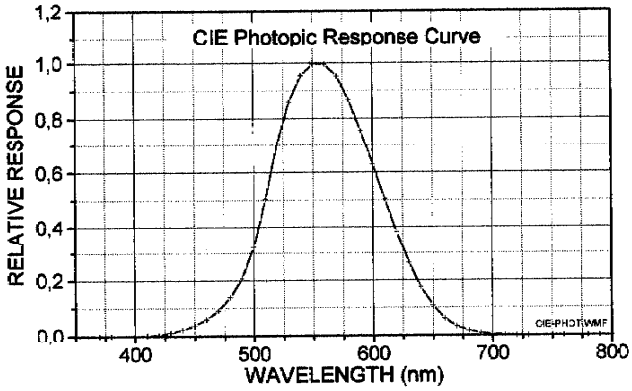


**Figure 3.20:** *The spectral response of a high quality lux-meter follows the CIE photopic response curve for the average human eye.*

The response measured by a radiometric instrument is determined by the incident spectral irradiance $I(\lambda)$, the spectral responsivity $R(\lambda)$ of the instrument and the transmittivity $T(\lambda)$ of any filter which may be interposed between the light and the detector. The instrument readout value $U$ in e.g. millivolts can be computed when these characteristics are known and the appropriate units are used for all quantities:

$$U = \int_{\lambda_1}^{\lambda_2} I(\lambda) \cdot R(\lambda) \cdot T(\lambda)\, d\lambda \qquad (3.6)$$

Schott Glaswerke provides $T(\lambda)$ data for its filters in tabular, graphical and digital form. We have used a selection of filters with cutoff wavelengths in the region from 375 - 850 nm. All quantities in the above equation are thus known except for the spectral irradiance $I(\lambda)$ from the light source to be studied. It is of interest to note that we are faced with an integral equation containing an unknown function, i.e. precisely the Fredholm integral inversion problem which will be encounter when extracting the aerosol size distribution to be described later in this thesis.

A spreadsheet has been used to tabulate the known information along with a column containing the irradiance $I(\lambda)$ which follows a Planck function with the color temperature $T$ as a parameter. It is now possible to compute the integral for a variety of assumed temperatures $T$ and to thus reach a computed value for each Schott filter of the expected lux-meter response for a light source with these Planck temperatures. On the other hand we can actually measure the instrument response using 15-20 different filters and compare our results with the computed values.

If the computed values are plotted against the measured values, a straight line should result, provided the assumed Planck temperature is correct. If the actual light source color temperature differs, then a curved line will result. Figure 3.21 shows an example of this analysis performed for a lamp with a color temperature of about 3000 K, but assuming temperatures of 2000, 3000 and 4000 K.

In order to have an objective criterion for when the line was "most straight" the sum of the residuals $\Sigma_i (U_M - U_P)_i$ was computed and plotted for a plausible range of color temperatures. The results are shown in Figure 3.22 and 3.23 for the noontime Sun in Denmark in August (Rayleigh air mass 1.3) and for a halogen lamp used for calibration.

The residuals plot equals zero for Sun and lamp color temperatures of 5850 K and 2710 K respectively, both reasonable values.

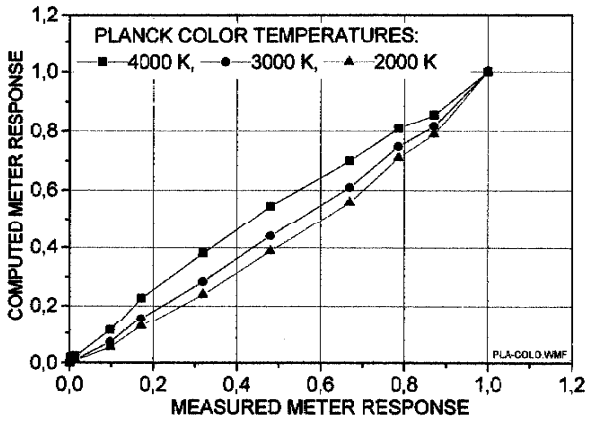


**Figure 3.21:** *Instrument response agrees best with the measured response for a Planck temperature of about 3000 K.*

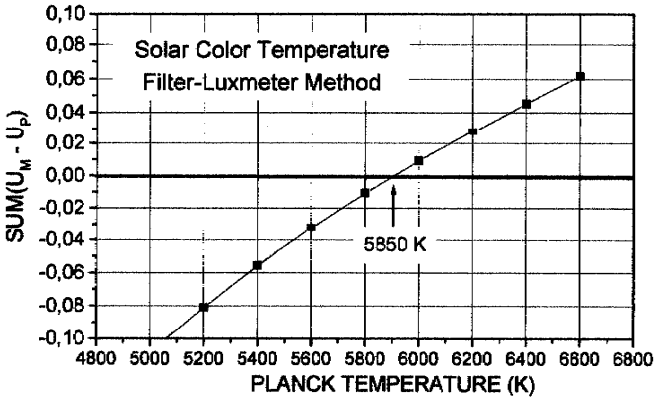


**Figure 3.22:** *Residuals for determination of the color temperature of the noontime sun.*

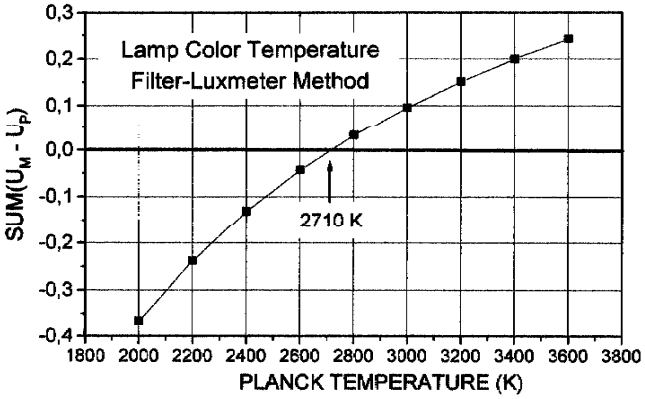


**Figure 3.23:** *Residuals for determination of the color temperature of a calibration lamp.*

## TRUE SOLAR SPECTRA

The final test of whether all efforts at calibration bear fruit is to check the solar spectrum itself under actual field conditions. The results of such measurements on a clear summer day near Silkeborg (August 1st, 1999) at location (56.10°N, 9.58°E) are shown in Figure 3.24.

Some of the most important absorption bands are summarized in Table 3.2 and many can be identified in the spectra shown in Figure 3.24. It is instructive to compare the spectra in this figure with the extraterrestrial solar spectrum shown in Figure 1.7 in Chapter 1.

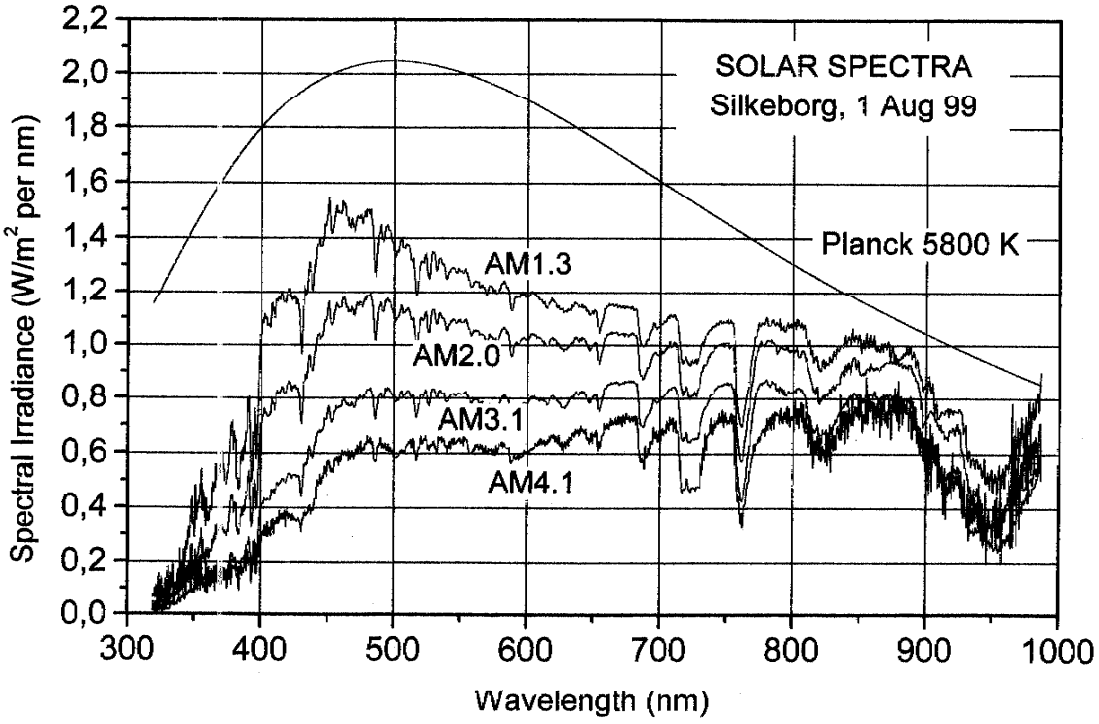


**Figure 3.24:** *The Planck function describing the extraterrestrial solar spectral irradiance (upper curve) and data for a range of air masses during August 1st, 1999, a clear summer day in Denmark (56.1°N). The upper data is for AM1.3 showing the noontime spectrum followed by graphs for AM2.0, 3.1 and 4.1. For main features see Table 3.2.*

| constituent | wavelength bands (approximate) | comments |
|---|---|---|
| ozone | 300-315 nm, 440-740 nm | Huggins, Chappuis band |
| oxygen | 759-763 nm | |
| water vapor | 690-694 nm, 717-721 nm<br>810-814 nm, 850-980 nm | vary with humidity |

**Table 3.2:** *Some of these major absorption bands are apparent in the solar spectral data.*

A wealth of information is available from solar spectra such as these. The absorption bands for ozone and water vapor can reveal important information about the ozone layer and the atmospheric moisture content. For a given wavelength outside a major absorption band semilogarithmic Langley plots (of instrument response vs. Rayleigh air mass) can be used in a manner analogous to the Langley plots from filter instruments to reveal the aerosol optical depth as a function of wavelength as described in Chapter 6.

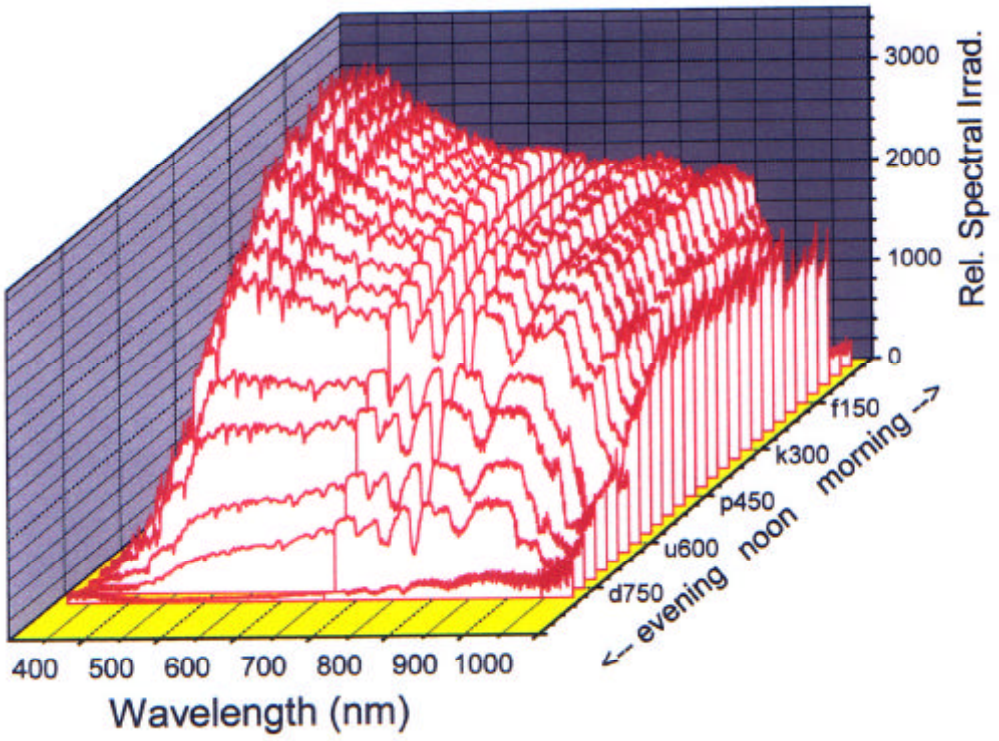


**Figure 3.25:** *Solar spectra collected at 30 minute intervals in Silkeborg during 1 August 1999. The spectra have been corrected using the instrument function as described. Note that red and near infrared wavelengths (600-1000 nm) predominate early and late in the day. During the middle of the day blue-orange wavelengths (400-600 nm) predominate.*

For completeness it is also appropriate to mention here the wavelengths recommended by WMO (World Meteorological Organization) for studies of atmospheric aerosol. These wavelengths have been selected to facilitate comparisons of data obtained from different locations and to avoid interference from molecular absorption bands. These recommended wavelengths are shown in Table 3.3. Four of these wavelengths were chosen for the pyrheliometers used in our experiment at Thule Air Base.

| Ultraviolet | Visible | Near Infrared |
|---|---|---|
| **368** nm | 440, **500**, 610, 675 nm | 778, 862, **1030**, 1250, **1550**, 1725, 2230 nm |

**Table 3.3:** *WMO recommended wavelengths for atmospheric aerosol studies. The wavelengths examined by our filter pyrheliometers were 368, 500, 1030 and 1550 nm.*

## APERTURE SIZE AND DIFFUSE LIGHT

An ideal direct incidence pyrheliometer would point directly at the solar disc (which subtends an angular arc of about 0.5°), and the aperture would permit only the direct rays from the Sun to reach the detector. This would place very high demands on the tracker. Therefore, the pyrheliometer aperture will often be selected with an opening angle of a few degrees, so that a small margin of tracking error is permissible, but with the disadvantage of allowing some scattered, diffuse light to be detected.

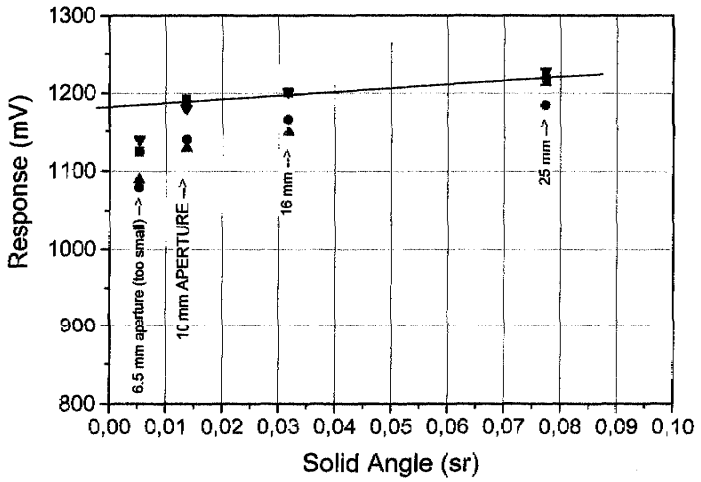


**Figure 3.26:** *A range of apertures were used to evaluate the effect of diffuse light on pyrheliometer response. The 10 mm aperture was selected.*

Russell et al. [*Russell, 1993, p 22971*] developed diffuse light correction factors for instruments used in their work. This correction procedure depends not only on the field of view but also on the ratio of large to small particles, the optical depth, the air mass and the wavelength. Their airborne sunphotometer had a full angle field of view of 4.4°, and the CMDL device on Mauna Loa had 2.3° field of view, which is comparable to the field of view of our instruments. Russell's optical depth correction factor is typically ½-1%. To evaluate this effect, we have performed the measurements shown in Figure 3.26. These measurements show the variation in instrument responsivity for a range of aperture sizes. Based on this test, which shows the error introducted by diffuse light to be minimal, and the work of Russell we have not performed any systematic corrections for diffuse light.

## SUMMARY

In this chapter we have described the mechanical and electrical configuration of the three SolData filter pyrheliometers and short wave pyrheliometer mounted for data collection at the Thule Air Base laboratory. We have also described the use of a CCD spectrometer for obtaining solar spectra including handling of wavelength calibration and coupling of the fiber optic cable to the entrance slit. The problem of calibration for correct measurement of the solar spectral irradiance with using a halogen calibration lamp in conjunction with each day of measurements was suggested as a solution. It has also been demonstrated how the correct color temperature of the calibration lamp can be determined using a true lux-meter and a selection of high-pass Schott filters. Finally, we have described check measurements to estimate the effects of scattered, diffuse light on our data.